PART I

COORDINATION CHEMISTRY IN NATIVE PROTEIN CAGES

1

THE CHEMISTRY OF NATURE'S IRON BIOMINERALS IN FERRITIN PROTEIN NANOCAGES

Elizabeth C. Theil and Rabindra K. Behera

1.1 INTRODUCTION

Ferritin protein nanocages, with internal, roughly spherical cavities ∼5–8 nm diameter, and 8–12 nm external cage diameters, synthesize natural iron oxide minerals; minerals contain up to 4500 iron atoms, but usually, in normal physiology, only 1000–2000 iron atoms are present; in solution the cavity is filled with mineral plus buffer. The complexity of protein-based iron-oxo manipulations in ferritins, which are present in contemporary archaea, bacteria, plants, humans, and other animals, is still being discovered [1]. Such new knowledge indicates that current applications exploit only a small fraction of the ferritin protein cage potential. To date, applications of ferritin protein cages to nanomaterial synthesis have been mainly as a template [2–4], and as a catalyst surface [5, 6]; some applications of ferritins as nutritional iron sources and targets or chelators in iron overload are also developing [3, 4].

There are two biological roles of the ferritins: concentrating iron within cells as a reservoir with large concentrations of iron for rapid cellular use, as in red blood cells (hemoglobin synthesis) or cell division (doubling of heme and FeS protein content), and for recovery from oxygen stress (scavenging reactive dioxygen and ferrous iron released from damaged iron proteins). Equation 1.1 shows the simplified forward reaction of ferritin protein nanocages.

$$2\mathrm{Fe(II)} + \mathrm{O_2} + 2\mathrm{H_2O} \rightarrow \mathrm{Fe_2O_3\,H_2O} + 4\mathrm{H^+} \tag{1.1}$$

Coordination Chemistry in Protein Cages: Principles, Design, and Applications, First Edition.
Edited by Takafumi Ueno and Yoshihito Watanabe.

In ferritin protein nanocages, the Fe/O reactions occur over distances within the cage of ∼50 Å (ion entry channels/oxidoreductase sites/nucleation channels/mineralization cavity) and over time spans that vary from msec (ferrous ion entry, active site binding, and reaction with dioxygen) to hours (mineral nucleation and mineral growth). Moreover, the reaction can be reversed by the addition of an external source of electrons, to reduce ferric to ferrous, and rehydration to release ferrous iron from the mineral and the protein cage. Exit of ferrous iron from dissolved ferritin minerals is generally slow (minutes to hours) but is accelerated by localized

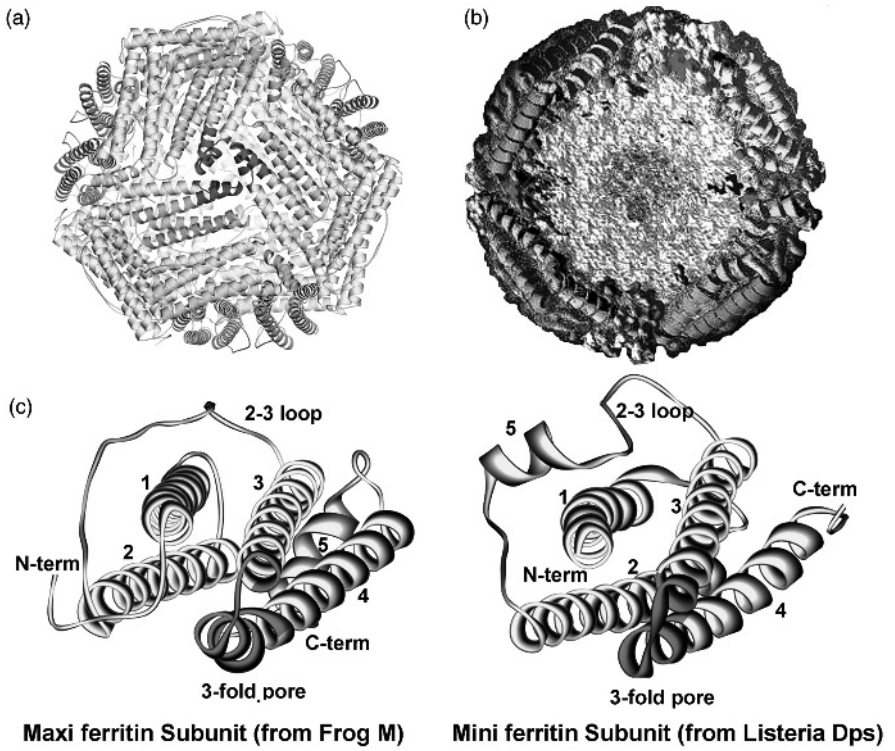

FIGURE 1.1 Eukaryotic ferritin protein nanocages and structural comparison of maxi- and mini-ferritin subunit. (a) An assembled 24-subunit ferritin protein with symmetrical Fe(II) entry/exit site at threefold pores (dark gray) that connects the external medium to inner protein cavity. Reprinted with permission from Reference 24. Copyright 2011 Journal Biological Chemistry. (b) Cross-section of ferritin protein cage (PDB:1MFR); sketch (gray cavity) showing filled ferric oxide mineral; arrow pointing ion channels. Reprinted with permission from Reference 12. Copyright 2010 American Chemical Society. (c) The 4-α-helix bundle (subunit) of maxi- (left) and mini-ferritin (right) drawn by us using PYMOL and the PDB files indicated; the fifth short helix is at the end of 4-α-helix and in 2-3 loop in maxi- (PDB:3KA3) and in mini-ferritin (PDB:2IY4), respectively, that defines fourfold and twofold symmetry upon self-assembling. The threefold pore regions that are conserved in both maxi- and mini-ferritin are shown in dark gray.

protein unfolding around the cage pores (Fig. 1.1), mediated by amino acid substitution of key residues in the ion channels or adding millimolar amounts of chaotrope [1, 7].

Ferritin proteins are so important that the genetic regulation is unusually complex. For example, in addition to ferritin genes (DNA), mRNA is also regulated by metabolic iron, creating a feedback loop where the catalytic substrates ferrous and/or oxidant are also the signals for ferritin DNA expression, ferritin mRNA regulation, and ferritin protein synthesis [8]. The iron concentrates in ferritins are used when rates of iron protein synthesis are high or, in animals, after iron (blood) loss. Rates of synthesis of iron proteins are high, for example, in preparation for eukaryotic cell division (mitochondrial cytochromes), plant photosynthesis (ferredoxins), plant nitrogen fixation (nitrogenase and leghemoglobin synthesis), red blood cell maturation (synthesizing 90% of cell protein as hemoglobin), immediately after birth, hatching, or metamorphosis (animals liver ferritin), and germinating legume seeds. After oxidant stress, ferritins play an important role in recovery, and in pathogenic bacteria in resistance to host oxidants by removing from the cell cytoplasm potent chemical reactants, ferrous ion and dioxygen or hydrogen peroxide. Protein-based catalytic reactions use Fe(II) and O to initiate mineralization of hydrated ferric oxide minerals.

The family of iron-mineralizing protein cages is apparently very ancient since they are found in archaea as well as bacteria, plants, and animals as advanced as humans. All ferritins share the following:

1. unique protein cavities for hydrated iron oxide mineral growth;
2. unusual quaternary structure of self-assembling, hollow nanocages with extraordinary protein symmetry (Fig. 1.1);
3. catalytic sites where di-Fe(II) ions react with dioxygen/hydrogen peroxide to initiate mineralization;
4. subunit protein folds in the common 4-α-helix bundle motif;
5. ion entry pores/channels;

Ferritin protein cages have variable properties as well:

1. cage size (subunit number: $n = 12$ or 24);
2. amino acid sequence: conserved among eukaryotes but divergent among eukaryotes, bacteria, and archaea (>80%) [9];
3. hydrated iron oxide mineral crystallinity and phosphate content;
4. catalytic mechanism for mineral initiation;
5. location/mechanism of mineral nucleation.

In this chapter we discuss protein cage ion channels, ferritin inorganic catalysis, and protein mineral nucleation and growth to provide fundamental understanding of ferritin structures and functions. The protein nanocage itself and the protein subdomains can be developed for templating nanomaterials, synthesizing nanopolymers

with fixed organometallic catalysts, producing nanodevices, and delivering nanosensors and medicines. The current status of such applications of ferritin cages are discussed extensively in Sections 1.2, 1.3, and 1.4.

1.2 FERRITIN ION CHANNELS AND ION ENTRY

1.2.1 Maxi- and Mini-Ferritin

Ferritins are hollow nanocage proteins, self-assembled from 24 identical or similar subunits in maxi-ferritins and 12 identical subunits in mini-ferritins that are also called Dps protein (*DNA-binding proteins from starved cells*) [10]. Cavities in the center of the protein cages account for as much as 60% of the cage volume. Cage assemblies from the 4-α-helix bundle protein subunits have 432 symmetry (24 subunits) or 23 symmetry (12 subunits) [11]. The unusual symmetry has functional consequences for ion entry and exit, and in the larger ferritins for protein-based control over mineral growth. Ferritin subunits are 4-α-helix bundles, ∼50 Å long and 25 Å wide (Fig. 1.1), that use hydrophobic interactions for helix and cage stability; charged residues on surfaces enhance cage solubility in aqueous solvents and ion traffic into, out of, and through the protein cage.

Ion channels with external pores are created around the threefold cage axes by sets of helix-loop-helix segments at the N-terminal ends of three subunits in the assembled cages (Fig. 1.1). The channels, analogs to ion channels in membranes, are lined with conserved carboxylate groups for cation entry and transit from the outside to the inside; ion distribution to multiple active sites occurs at the interior ends of the channels [12]. Each channel, eight in maxi-ferritin cages and four in mini-ferritin cages, is funnel shaped [1, 12]. In maxi-ferritins, constrictions in the channel center may be selectivity filters. (Fig. 1.2). At the C-terminal end of ferritin subunits in maxi-ferritins, a second cage symmetry axis occurs, created by the junctions of four subunits that can form pores [13]. The region is primarily hydrophobic and the fourfold arrangement of nucleation channel exits contributes to mineral nucleation. In mini-ferritins, by contrast, the C-termini form pores with threefold symmetry [11, 14] that in some mini-ferritins can participate in DNA binding [15].

Maxi-ferritins are found in all types of higher organisms (animals and plants including fungi), and bacteria (ferritins and heme-containing bacterioferritins (BFRs)). Mini-ferritins, by contrast, are restricted to bacteria and archaea and may represent the transition of anaerobic to aerobic life, because of the ability to use dioxygen and/or hydrogen peroxide as the oxidant in the Fe/O oxidoreductase reaction. The secondary and quaternary structures of ferritins are very similar [10] in spite of very large differences in primary amino acid sequences.

The fifth helix in ferritin subunits, attached to the four-helix bundle, distinguishes maxi-ferritins (animal and plant H/M chains and animal L chains, bacterial ferritins, and the heme-containing bacterioferritins) from the smaller mini-ferritin (Dps proteins). In maxi-ferritins, helix 5 is at the C-terminus, positioned along the fourfold symmetry axis, at ∼60° to the principal helix bundle. A kink in helix 4 occurs at

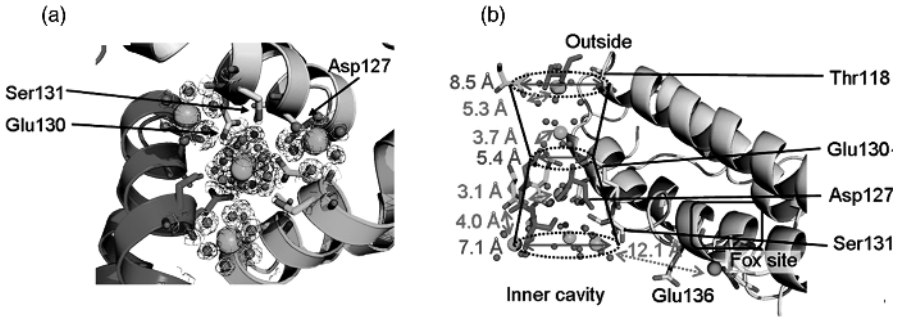

FIGURE 1.2 Iron entry route in ferritin. Fe(II) ion channels showing a line of metal ion (Big spheres) connecting from the outside to inner protein cavity (PDB:3KA3). Adapted with permission from Reference 12. Copyright 2010 American Chemical Society. (a) A view from inside the cavity through the channel toward the cage exterior, showing three metal ions at the exit into the cavity; they are symmetrically oriented toward each of the catalytic centers in the subunits that form the channel by binding to one of the Asp127 residues in each subunit. The fourth metal ion in the center is the end of the line of metal ion stretching from the external pore through the channel to the cavity. (b) The conserved negatively charged residues in one subunit that defines the ion channel are shown as sticks. Big spheres are Mg(II) and small spheres are water molecules; a ∼4.5 Å diameter constriction is at the center of the channel at Glu 130.

the position of an aromatic residue (Tyr/His/Phe 133), which sterically alters the helix at the point where localized pore unfolding stops [16, 17]. Mini-ferritins (Dps proteins), by contrast, lack the fifth helix at the C-terminus; some have helices in the loop connecting helices 1 and 2 as in the mini-ferritin cage of *Escherichia coli*, and Dps proteins (Fig. 1.1) where helix 5 participates in subunit–subunit interactions along the twofold axes of the cage. In most of the maxi-ferritins, the di-iron oxidoreductase (ferroxidase or F_{ox}) center is located in the central region of the four-helix subunit bundle and is composed of residues from all four helices of the bundle. In spite of the structural differences between maxi- and mini-ferritins and the large sequence differences (>80%), all ferritins remove Fe(II) from the cytoplasm, catalyze Fe(II)/O oxidoreduction, provide protein-caged, concentrated iron reservoirs, and act as antioxidants [10, 11].

1.2.2 Iron Entry

Central to the understanding of ferritin iron uptake and release is the route of iron ion entry and exit through the protein cage. Both the theoretical (electrostatic calculations) and experimental (x-ray crystal structure, site-directed mutagenesis) studies of different ferritins converge on the ion channels around the threefold cage axes as the iron-uptake route (Fig. 1.2). Early x-ray crystal structures [18, 19] and electrostatic calculations indicated iron entry along the 12 Å long hydrophilic threefold channels. Recently, a line of metal ions in the channel was observed in ferritin channels (Fig. 1.2b) much like those in other ion channels [20] that connect the external

threefold pores to the internal cavity [12]. Electrostatic potential energy calculations describe a gradient along the threefold channels of maxi-ferritins that can drive metal ions toward the protein interior cavity [10, 21, 22]. Site-directed mutagenesis studies confirmed the role of the negatively charged residues both on oxidation [23] and on diferric peroxo (DFP) formation, where selective effects of different carboxylate groups were also observed [24]. In the mini-ferritin, *Listeria innocua* Dps (*Li*Dps), channel carboxylates also control iron oxidation rates that, in contrast to maxi-ferritins, also control iron exit rates [25]. A functional role of the threefold channel in transit of Fe(II) ions through the ferritin cage to and from the inner cavity of ferritin was indicated by crystallographic studies on many ferritins (human, horse, mouse, frog) where divalent metal ions (Mg^{2+}, Co^{2+}, Zn^{2+}, and Cd^{2+}) are observed in the channels [11, 12, 26, 27]. However, how the hydrated Fe(II) with diameter of 6.9 Å passes through the ion channel constrictions, diameter about 5.4 Å, (Fig. 1.2) is not known. A possible explanation might be fast exchange of labile aqua ligands of Fe(II) with the threefold pore residues [28] or dynamic changes in the ion channel structure or both.

1.3 FERRITIN CATALYSIS

Ferritin nanocage proteins sequester and concentrate iron inside the cell by iron/O_2 chemistry. In bacteria and plants, ferritins are usually found as homopolymers composed of H-type subunits whereas in vertebrates, they are heteropolymers of 24 subunits, comprising two types of polypeptide chains called the H and L subunits [10]. The ratios of H to L subunits are tissue specific, with more H subunits present in the heart whereas L subunit contents are more in the liver [10]. Ferritin H subunits possess catalytic, di-Fe(II)/O_2 oxidoreductase sites (ferroxidase/F_{ox}) at the center of the 4-α-helix bundle of each eukaryotic maxi-ferritin subunit that rapidly oxidize Fe(II) to Fe(III). By contrast, the L subunit possesses amino acid residues known as the nucleation sites that provide ligands for binding Fe(III); in this case, initiation of crystal growth and mineralization occurs on the inside surface the ferritin protein nanocage. Another type of ferritin subunit is found in the amphibians known as "M" type that closely (85% sequence identity) resembles the vertebrate H type [12, 29]. In this section structure–function relationships in ferritin catalysis in eukaryotic maxi-ferritins and characterizations of reactive intermediates are described. Detection of reaction intermediates in heme-containing bacterioferritins and mini-ferritins (Dps proteins) with hydrogen peroxide as the oxidant has been elusive.

1.3.1 Spectroscopic Characterization of μ-1,2 Peroxodiferric Intermediate (DFP)

Fe(II) ions from the solution move to the inner cavity of the ferritin nanocage through hydrophilic threefold channels. At the channel exits, on the inner surface of the protein cage, the ions are directed to each of the 24 oxidoreductase sites where oxidization to Fe(III) by dioxygen is completed. Transit and oxidation requires only milliseconds, whereas solid hydrated ferric oxide mineral formation takes many hours [13]. The

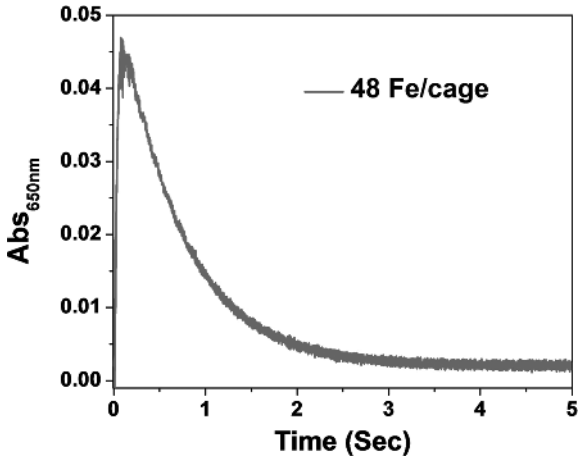

FIGURE 1.3 A typical time course of DFP formation and decay. The reaction conditions for 48 Fe(II)/cage are mixing of equal volumes of protein solution (4.16 μM wild-type frog M ferritin in 200 mM Mops, pH 7.0, 200 mM NaCl and 0.2 mM $FeSO_4$ solution in 1.0 mM HCl) in air (mixing time <10 msec) at 20°C (Π-Star, Applied Photophysics); absorbance values were measured at 650 nm, the λ_{max} for the DFP intermediate in the Fe(II)/O_2 oxidoreductase.

process of iron oxidation catalysis and biomineralization of ferritin core proceeds via complex mechanism of formation and decay of transient intermediate DFP (Eq. 1.2); a blue complex is observed by rapid-mixing, UV-vis spectrometry [30–32].

$$\text{Ferritin} + 2\text{Fe(II)} + O_2 \longrightarrow [\text{Fe(III)}{-}\text{O}{-}\text{O}{-}\text{Fe(III)}]^* \xrightarrow[-H_2O_2]{H_2O} [\text{Fe(III)–O(H)–Fe(III)}]$$
$$\longrightarrow (\text{Fe(III)}\text{–}\textit{O}\text{–Fe(III)})_{2-8} \longrightarrow (Fe_2O_3)\cdot(H_2O)_x + 4H^+ \qquad (1.2)$$

DFP ($\lambda_{max} = 650$ nm) is the first detectable intermediate during iron oxidation at the F_{ox} site of the ferritin. The complex has been characterized by a variety of spectroscopic analyses in frog M ferritin where DFP formation and decay kinetics are particularly favorable for DFP accumulation and spectroscopy (see Fig. 1.3) [33, 34]. Mössbauer parameters ($\delta = 0.62$ mm/s, $\Delta E_Q = 1.08$ mm/s), typical for ferric species but with diamagnetic ground state, indicated the presence of anti-ferromagnetic interaction [35]. Peroxodiferric complexes with similar Mössbauer parameters are also formed as early intermediates in the reaction of O_2 with human H ferritin and the catalytic di-iron non-heme proteins (Table 1.1). The formation and decay profiles of this transient intermediate obtained both by rapid freeze-quench (RFQ) Mössbauer and stopped-flow absorption spectroscopy were identical, and confirmed the formation of only single transient species in the solution mixture during that time regime. The molar extinction coefficient for this species was estimated to be $\sim$1000 $mM^{-1}cm^{-1}$ at 650 nm, using the results obtained by the two different methods mentioned above [33].

Information on the O-O bridge in DFP was obtained from RFQ resonance Raman and RFQ X-ray absorption studies. The detection of O-isotope sensitive bands

TABLE 1.1 Spectroscopic Parameters for the DFP Intermediates in Ferritin and Di-iron Carboxylate Proteins

	Optical Parameter		Mössbauer Parameter		Peroxide Binding	
Protein	λ_{max} (nm)	ε ($cm^{-1}M^{-1}$)	δ (mm/s)	ΔE_Q (mm/s)	Mode	Reference
Frog M ferritin	650	1000	0.62	1.08	μ-1,2	[30]
Human H ferritin	650	850	0.58	1.07	μ-1,2	[29]
sMMOH	725	1500	0.66	1.51	–	[36]
RNR-R2 D84E	700	1500	0.63	1.58	μ-1,2[a]	[37]
Δ^9-desaturase	700	1200	0.68; 0.64	1.90; 1.06	μ-1,2	[38]

[a]To trap DFP, amino acid substitutions D84E/W48F variant were used [37].
MMOH, methane monooxygenase; RNR-R2, ribonucleotide reductase R2; Δ^9-desaturase, Δ^9-stearoyl-acyl carrier protein desaturase.

assigned to ν(Fe-O) at 485 and 499 cm^{-1} and ν(O-O) at 851 cm^{-1} is consistent with a μ-1,2-bridging mode of the peroxide ligand as reported for different di-iron proteins [39]. An unusually short Fe-Fe distance (2.53 Å) in the μ-1,2 peroxodiferric intermediate was detected in the early steps of ferritin biomineralization by RFQ EXAFS spectroscopy [40], which is significantly shorter than those in other di-iron proteins such as R2 and sMMOH (3.1 to 4.0 Å). This short Fe-Fe distance (2.53 Å) was proposed to have stronger O-O bond and requires a small Fe-O-O angle (106° to 107°). The unique geometry in the ferritin catalysis was suggested to favor the decay of the DFP intermediate by the release of H_2O_2 and μ-oxo or μ-hydroxo diferric biomineral precursors instead of forming high-valent Fe(IV)-O species as in R2 and sMMOH that oxidizes organic substrate (Fig. 1.4).

Both ferritin and di-iron oxygenases are members of the di-iron-carboxlyte protein family [41]. While both share the same DFP, the decay paths are different. In ferritins, diferrous is a substrate, whereas in oxygenases, diferrous is a cofactor and is retained at di-iron sites throughout catalysis. The lability of diferrous ions in ferritin in air prevents direct identification of the F_{ox} site ligands in typical ferritin protein crystals. In Ca or Mg (ferrous analogs) ferritin cocrystals, longer metal–metal distances [11, 12, 29] were observed compared to iron–iron distances or ligands from solution EXAFS [40]; the ligand sets were also slightly different than for di-ferrous binding by VTVH MCD/CD [42].

Using protein chimeras, the iron sites (1 and 2) at the active centers required for DFP formation were positively identified when iron ligands proposed to be important for catalysis were inserted into catalytically inactive L ferritin [43]. Four of the six active site residues are the same in ferritins and di-iron oxygenases (except in heme-containing BFR with all six di-iron cofactor site ligands); ferritin-specific Gln137 and variable Asp/Ser/Ala140 (at Fe2) substitute for Glu and His, respectively, at di-iron cofactor active sites (Fig. 1.4a). The contrasting properties of ferritin or di-iron oxygenases, toward Fe(II) as substrate or cofactor, reflect differences in the amino acid residues at one of the di-iron sites in the catalytic centers. Amino acid residues (ligands) at Fe1 site are shared by ferritins and di-iron cofactor proteins. However, different and weaker Fe(II) ligands are present at Fe2 site in ferritin di-iron catalytic

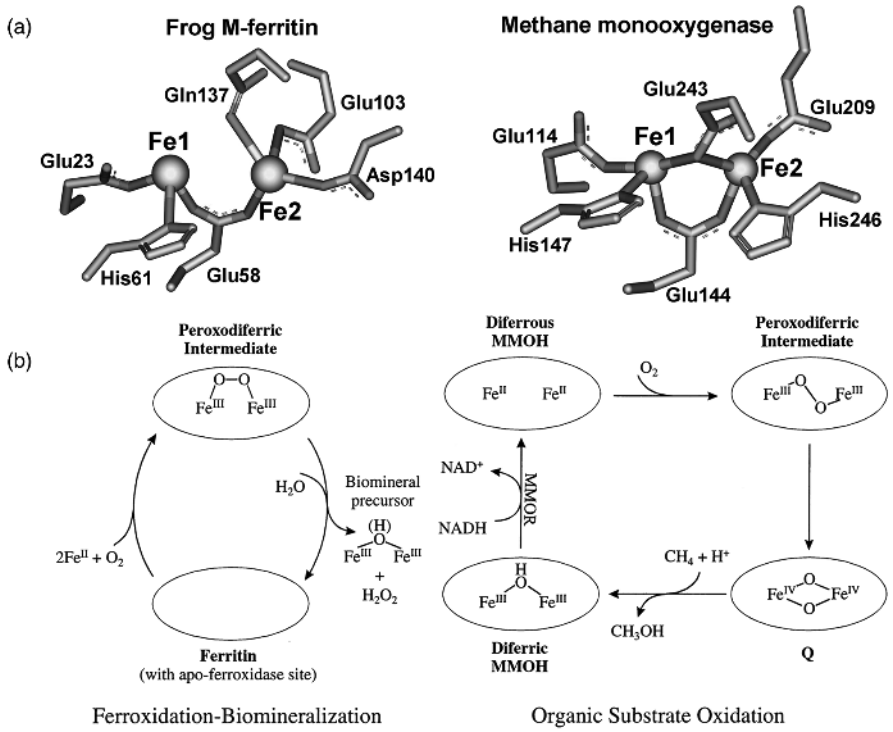

FIGURE 1.4 Comparison of the active site residues in the fate of peroxodiferric-protein (DFP) complexes during biomineralization (ferritin) and oxygen activation (MMOH). Reprinted with permission from Reference 40. Copyright 2000 AAAS. (a) Structures of the di-iron active sites in frog M-ferritin (1MFR) crystallized with Mg(II) as a Fe(II) homolog (left) and in di-iron cofactor site in MMOH (1FYZ) (right). Note the activity-specific ligands in the Fe2 site; ferritin specific: Gln (137) and Asp (140) are replaced by Glu (243) and His (246), respectively, in MMOH that decides the function of DFP intermediate. (b) Comparison of the fate of peroxodiferric-protein complexes during biomineralization (ferritin) and oxygen activation (MMOH). Modified from Reference 44. In ferritin, the eukaryotic ferritin peroxodiferric complex decays to diferric oxo or hydroxo mineral precursors that move from catalytic sites into nucleation channels with the release of hydrogen peroxide (left). In MMOH, DFP decay produces a high valent oxidant (Q) that oxygenates organic substrates and forms the diferric cofactor which is reduced to the initial diferrous cofactor by the redox partner, MMOR (right).

centers which permit the release of diferric oxo products and entry into the nucleation channels. Residue Ala26, identified by covariation analysis, is between large numbers of catalytically active and inactive ferritin subunits proximal to the active site. Ala26 is critical in normal turnover and release of catalytic products (diferric oxo) into the nucleation channels of eukaryotic ferritins [24] and is replaced by Ser in some L subunits, which are catalytically inactive. The loss of flexibility around the active sites also coincides with the loss of activity [12, 44].

Within the ferritin superfamily, two alternatives to the eukaryotic Fe1 and Fe2 sites at catalytic centers are known. In mini-ferritins, catalytic centers have fewer iron ligands. The substrate iron is usually bound between by ligands contributed by two different subunits at the subunit dimer interface [15, 25]. In heme bacterioferritins, the Fe2 site is similar to the di-iron oxygenase cofactor sites; iron serves both as substrate and as cofactor in BFR.

1.3.2 Kinetics of DFP Formation and Decay

The iron oxidation product in all the ferritins absorbs in the range 300–420 nm; due to the Fe(III) oxy absorption, an unresolvable mixture of DFP, Fe(III) oxo/hydroxo dimer, and Fe(III) biomineral results. However, some ferritins, in addition to this absorption band, also exhibit a broad band in the range 600–720 nm, which arises due to the formation of DFP with absorption maxima around 650 nm [10, 31, 45, 46].

In the chimeric ferritin, the Fe1 site (e, ExxH) was insufficient for ferroxidase activity [43]. Both Glu-Glu-xx-His and Glu-Gln-xx-Asp were required. In wild-type ferritins, when both the ligand set of di-iron oxygenase cofactors were created by amino acid substitution (Fe2: Gln137→Glu or Asp140→His), catalytic activity (DFP formation) was destroyed and the Fe(III)O formation rate decreased 40-fold [44]. The kinetics of ferroxidase activity in ferritin with di-iron cofactors residues illustrates the importance of ferritin-specific residues in the Fe2 site in ferritin catalytic centers for the DFP formation and its decay to different species in ferritin and di-iron cofactor proteins as described earlier.

Conserved amino acid residues located at the threefold axis (Asp127 and Glu130) and residues distal to the active sites influence the kinetics of DFP formation and iron oxidation, in addition to the Fe site ligands at the active sites [24]. Positive cooperativity, sigmoidal behavior with increasing Fe(II) concentration, occurs in the formation of DFP and Fe(III)/O species. However, the Hill coefficient for the formation of DFP and Fe(III)/O species ($n \sim 1.7 \pm 0.2$) [43, 44] is smaller than that reported ($n \sim 3$) [42] for the binding of Fe(II) at F_{ox} site in the absence of oxygen [42–44]. The Hill coefficient of 3 indicates binding of Fe(II) at three oxidoreductase sites directed by three clustered carboxylate residues (Asp127) at the opening of the Fe(II) entry channels into the cavity of the ferritin protein cage around threefold axes of the cage. Since the cooperativity of Fe(II) binding was independent of di-Fe(II) binding at each of the active sites and occurred in the absence of oxygen, protein–protein interactions involving three subunits were indicated. In the presence of dioxygen, cooperativity might differ. However, in Asp127A ferritins, cooperativity is eliminated ($n \leq 1$) indicating the role of Asp127 in the previously observed cooperativity (R. Behera and E.C. Theil, to be published). The mechanism of iron oxidation is well studied, but the DFP decay pathway/kinetics are unknown; changes in decay kinetics by amino acid substitutions occur by changing residues at the active sites—residue 140 [44], iron transport residues 26, 42, and 149 [24], and Fe(II) substrate concentrations (R. Behera and E.C. Theil, to be published).

H_2O_2 generated during initial F_{ox} reactions, when the total ferritin iron content is low, is released into solution; diferric oxymineral precursors leave the active sites

traveling through the protein to the protein cavity. The generation of free radicals by the so-called Fenton reaction between the DFP decay products, such as H_2O_2, and substrates, such as Fe^{2+}, is very low in ferritin as they are spatially separated by the protein during turnover. The mechanism of DFP decays to diferric mineral precursors and H_2O_2 is not known, but hydrolysis of DFP has been proposed to be involved. At low ratios of iron : protein, H_2O_2 generated during DFP decay was correlated quantitatively with the amount of DFP accumulated at 70 ms, determined by RFQ Mössbauer spectroscopy [47]; DFP decayed to H_2O_2 with 1 : 1 stoichiometry at or below 36 Fe(II)/cage. Multiple diferric oxo species were detected by RFQ Mössbauer spectroscopy and found to decay very slowly to mineral, suggesting the existence of multiple stages in the pathway between DFP and the diferric hydroxo and H_2O_2 products.

Protons ($2H^+$/Fe) generated by hydrolysis of water, coordinated to ferric ions during catalysis/mineral nucleation/mineral growth, diffuse from the protein to the solution. Still unknown is how the diferric oxo reaction products are propelled into and along the nucleation channels (Fig. 1.5a). Possibly changes in acidity of water coordinated to iron during oxidation contribute to di-Fe(III)O release. The long catalytic turnover times [30, 48] and the hours required for the stabilization of ^{13}C–^{13}C NMR NOESY spectra after each addition of saturating amounts of Fe(II) substrate [13] both suggest slow, reversible, likely local, conformational (helix unfolding/folding?) changes are occurring during diferric oxo product release and mineral nucleation.

In some bacterial ferritin, such as the Dps proteins that protect DNA against the oxidative damage, the putative F_{ox} site is on the inner surface of the protein cavity at the dimer interfaces, rather than in the center of each subunit, as seen in eukaryotic ferritin. Although both types of ferritin make iron minerals, a property of Dps proteins is the preferential use of H_2O_2 as the iron oxidant (Eq. 1.3) during ferritin core formation [10].

$$2Fe^{2+} + H_2O_2 + (H_2O)_{x+1} \rightarrow [?] \rightarrow Fe_2O_3(H_2O)_x + 4H^+ \qquad (1.3)$$

1.4 PROTEIN-BASED FERRITIN MINERAL NUCLEATION AND MINERAL GROWTH

Ferritin minerals naturally vary in average size, phosphate content, and crystallinity depending on the cytoplasmic environment. The average mineral size in ferritins isolated from natural tissues represents a distribution of mineral sizes, which coincides with a distribution of densities within a s ample of the protein mineral complex. The number of iron atoms/cage mineral can vary from zero (“apoferritin”) to many thousands. Sub-fractions of ferritin, varying in both mineral size and cross-links between protein cage sub units, can be purified from natural ferritin preparations by sedimentation in sucrose gradients. When iron mineral from natural tissue ferritin isolates is dissolved and the iron mineral is reconstituted in apoferritin (empty protein cages) *in vitro*, the distribution of ferritin mineral sizes is more narrow than the mineral sizes present in natural tissue ferritins [49, 50]. Why mineral sizes vary among ferritins

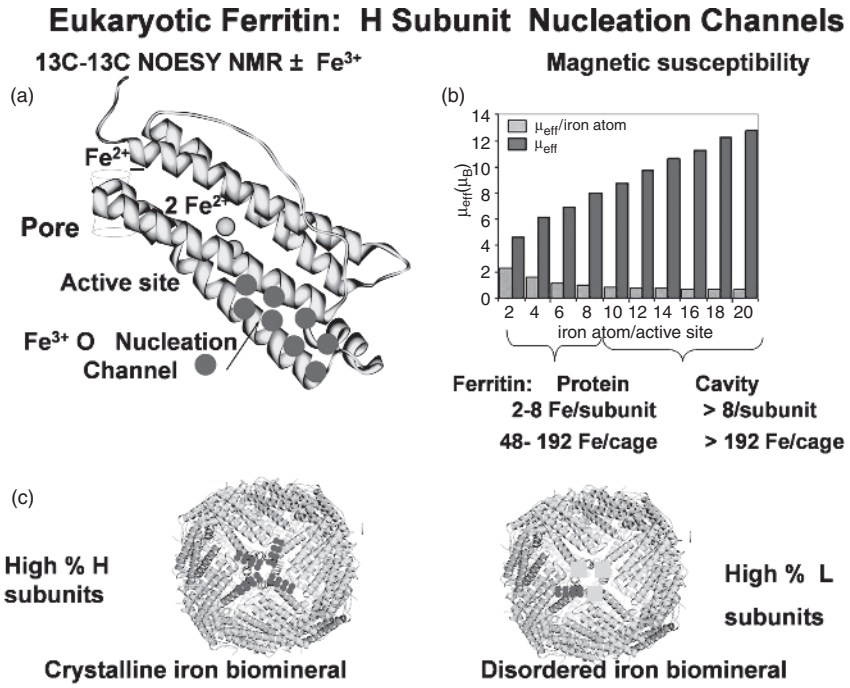

FIGURE 1.5 Protein-based control of iron biomineral order in eukaryotic ferritins. (a) Location of Fe(III) during multiple oxidoreductase turnover cycles at ferritin active sites, determined by residue broadening in ^{13}C–^{13}C solution NOESY; note that four Fe(II) catalytic cycles/active sites, are required for iron to reach the cavity entrances Adapted with permission from Reference 1. Copyright 2011 Curr Opin Chem Biol. (b) Changes in Fe(III)O magnetic susceptibility of growing ferritin mineral precursors inside the nucleation channels during multiple turnovers at the active sites. Reprinted with permission from Reference 13. Copyright 2010 Proc. Nat'l Acad. Sci. U.S.A. (c) An illustration of proximity effects for multiple H (catalytically active) or multiple L (catalytically inactive) animal ferritin subunits on organized mineral nucleation and biomineral growth, drawn using Pymol and PDB file 1MFR.

from *in vivo* sources remains unknown, but is likely the results of complex variations in iron delivery and iron utilization as well as subcellular distributions of ferritins in different tissue/cell types.

Ferritin minerals with a high phosphate content relative to iron, as in bacteria and plants (Table 1.2), are amorphous. The phosphate content of the bacterial cytoplasm and plant plastids, which have endosymbiotic ancestors that were single-celled organisms [51], is relatively high. If ferritin protein cages isolated with more ordered minerals are demineralized and reconstituted in solution with minerals in the presence of large amounts of phosphate, the minerals are disordered [52, 53], indicating the role of the mineralization environment on mineral structure. In the case of plants, ferritin is synthesized in the cytoplasm but is targeted to the high-phosphate plastids. Such observations, combined with the amorphous, high-phosphate structure of plant

TABLE 1.2 Natural Variations in Ferritin Average Mineral Sizes and Phosphate Content

Ferritin Source	Mineralized Ferritin Iron, (Average Number Atoms/Cage)	Ferritin Mineral-Iron : Phosphate (Moles/Mole)	Reference
Human thalassemic liver	2500	2 : 1	[37]
Horse Spleen	2000	8–10 : 1	[55]
Pea[a]	1800–2000	2.8 : 1	[51, 52]
Azotobacter Vinelandii	800–1200	1.5–1.9 : 1	[47]
Pseudomonas Aeruginosa	700	1.7 : 1	[56]
E. coli heme-ferritin (BFR)	25–75	1.4–2.2 : 1	[57]

[a]Plant ferritins are sometimes called phytoferritins because of the biological source [58]. However, structurally, plant ferritins vary in sequence only 40% from animals and are clearly in the eukaryotic ferritin family, contrasting with the 80% sequence divergence between bacterial and eukaryotic ferritins [9].

ferritin minerals has led to the conclusion that in plants, ferritins are mineralized inside the plastid [52, 53].

Minerals in ferritin protein cages from animal tissues can be either disordered or relatively ordered even though the mineral phosphate content is relatively constant [52, 54]. Recent evidence suggests that the control of mineral order in animal ferritins is an inherent property of the protein cages. In a study of the amino acids that were near Fe(III) during ferritin mineral nucleation, a previously unknown channel was discovered [13]. In the channel, the diferric oxy products of ferritin catalysis from each active site interact during multiple catalytic turnovers, forming tetrameric ferric oxy species and larger. The mineral nuclei are dispersed within the channels, apparently linearly along the 20 Å channel, and emerge at exits into the cavity around the fourfold symmetry axis of the cage. As many as eight Fe(III) ions are required to reach the end of the cavity, suggesting that iron mineral nuclei of significant size emerge into the cavity of the protein cage (Figs. 1.1, 1.5). Each nucleation channel exit is near the exits of three other subunits around the fourfold symmetry axes of the protein cage (Figs. 1.1, 1.4), which facilitate the ordered interactions of mineral nuclei from four subunits and the buildup of highly ordered ferritin minerals.

If mineral nuclei from each active site are directed through intra-cage nucleation channels to exits from four subunits that are symmetrically clustered to form ordered minerals, how then do animals form less ordered ferritin mineral observed [54] in some tissue? The answer appears to reflect a unique gene product in animal ferritins, the L subunit which is encoded in an apparently duplicated/modified H ferritin gene; L subunit deficiencies are related to changes in cell proliferation [59]. L subunits are catalytically inactive and lack some of the residues required for catalysis, such as Glu23 and Gln137 (Fig. 1.4a), and also the residues required for protein-channel nucleation, such as Ala26 [24]. H and L subunits spontaneously self-assemble into cages with the ratio of H : L subunits genetically controlled and varied for each

animal tissue. In the liver, for example, ferritin protein cages have a large number of catalytically inactive L subunits and a relatively small number of catalytically active H subunits, whereas in the heart, ferritin proteins predominately have H subunits. Since there are few catalytic sites and few nucleation channels in a ferritin rich in L subunits, as in liver, the ferritin mineral should be poorly ordered (Fig. 1.5), as is, in fact, the case [54]. In the high H subunit ferritin from heart, where there are many catalytic sites and nucleation channels in each cage, multiple mineral nuclei will emerge in the cavity near mineral nuclei from many other subunits (Fig. 1.5c,d), leading to a highly crystalline mineral, which indeed it is [54]. The physiological advantage of tissue-specific ferritin minerals in animals with different degrees of order is not understood, but may relate to the rates of mineral dissolution and/or local dioxygen concentrations. Liver ferritin is a reservoir of iron for the entire body, recruiting iron quickly for distribution to other tissue, for example, after blood loss when increased synthesis of new red blood cells (hemoglobin and iron-rich) is required. A disordered mineral in the L-subunit-rich liver ferritin may dissolve more quickly in response to the sudden biological iron need. Conversely, heart ferritin, which accumulates highly crystalline minerals in the H-subunit-rich heart ferritin may reflect the antioxidant properties of ferritin minerals in cells that have high, local dioxygen concentrations and need to sequester iron more tightly until regulated opening/unfolding of the ion channel exit pores [1].

1.5 IRON EXIT

Regulating iron entry/exit channels can be important in the application of ferritin cages to nanochemistry and nanotechnology, and is also important for the growth and the survival of living organisms. *In vivo* iron release from ferritin and turnover of the empty protein cages is complex; it occurs in at least two sites within the cells: proteasomes, the supramolecular protein complexes that mediate ferritin cage and other protein degradation in the cytoplasm after iron is released; and lysosomes, acidic, subcellular compartments with hydrolytic enzymes and membrane pumps to transport to the cytoplasm after degradation of the protein cages [10, 60]. Required to dissolve ferritin minerals under physiological conditions, based on solution studies, are reductants, thought to be $FMNH_2$, protons, water for ion rehydration, and external Fe(II) transporters that are yet to be identified.

Localized changes in ferritin protein cage structure contribute significantly to the rates of Fe(II) exit from the caged ferritin minerals and regulate the rates of ferritin mineral reduction and rehydration. The Fe(II) ion entry channels, formed by helix-loop-helix motifs at the threefold symmetry axes of the cage, are also the Fe(II) exit channels. However, in contrast to the use of negatively charged residues and constrictions to propel cations into the cage [10, 22], residues controlling the rates of mineral dissolution in eukaryotic ferritins are more involved with helix folding/unfolding. Localized unfolding in ferritin protein cages is controlled by hydrophobic amino acids such as leucine, an arginine–aspartate salt bridge [16, 17, 61, 62], and by the

addition of external chaotropes such as urea or guanidine [7]. Heptapeptides, identified as binding, from a combinatorial library can either increase or decrease localized folding and Fe(II) release from ferritin minerals [63]. Conserved Arg72 and Asp122, which form salt bridges at the openings of the ion channels, and conserved Leu110 interact with conserved Leu134 deep in the channels; all have a significant impact on folding of the threefold channel; Glu130 and Asp127 by contrast have no effect on iron exit but control ion entry.

The N-terminal extension of the 4-α-helix bundle lies near the external opening of the ion entry pores. Substitutions Arg72Asp and Asp122Arg increase mineral dissolution and Fe(II) exit [62]. In protein crystal structures of ferritin M Arg72Asp, the N-terminal extension is completely disordered apparently because of disruption the H-bond network between Gln5/Arg72, which is linked to loop Asp122 by a salt bridge; protein crowding restores normal function [64]. Such studies show that the N-terminal extensions of the ferritin four-helix bundles act as exit gates for the ion pores in eukaryotes and contrast sharply with mini-ferritins where negatively charged residues appear to control both cation entry and exit [25]. Such variety in ion channel function and control between maxi- and mini-ferritins should find useful applications of ferritin cages in nanoscience.

1.6 SYNTHETIC USES OF FERRITIN PROTEIN NANOCAGES

Ferritin protein nanocages are currently used in a number of applications that are briefly summarized here and described in detail elsewhere in the book. Examples include catalysis [5, 65, 66] (Chapter 7), templating of nanoparticles/materials [2, 4, 6, 67], delivery of imaging agents [3, 4, 67] (Chapter 11), and nanoelectronics [68, 69] (Chapters 11–12). Among the metal ions used in ferritin-based catalysts or materials are Au, Pd, Rh ions Pt, Ni, Cr, CdS, Ti, Eu, Ti, Co, and Fe [2, 67].

The unusual protein stability of ferritin cages means ferritin protein cages can be used under relatively extreme conditions. Ferritin is naturally stable in aqueous solutions (heat up to 80 °C), chaotropes such as 6 M urea or guanidine (at pH 7), and detergent such as 1% sodium dodecyl sulfate (SDS) [70]. However, coupling of long chain hydrocarbons (C9, C12, C14) allows reversible dissolution of intact ferritin proteins cages in organic solvents such dichloromethane, ethyl acetate, and toluene [71], and low pH/high pH disassembly/assembly has allowed entrapment in aqueous systems [72].

Availability of many natural metal-binding sites in ferritin, provided by the disproportionately large fraction of amino acid side chains with negative charges (over 700/24 subunit maxi-ferritin cage), makes ferritin cages particularly attractive for metallocatalysts and nanomaterials. During the natural function of ferritin, such sites are important in cage transport of iron ions (Fe^{2+}), binding the catalytic substrate (di-Fe^{3+})O, and binding the catalytic product and mineral precursors. Many nanochemistry/nanomaterial studies use a commercially available ferritin rich in L subunit [2] catalytic centers and mineral nucleation channels and is specific to animals.

Ferritin L subunits, specific to animals, lack residues for the natural Fe^{2+}/O_2 catalysis and for $Fe^{3+}O$ transport and appear to be important in regulating iron mineral order [1, 24]. In addition, new functional iron-ferritin protein sites are still being discovered in ferritin [13, 24]. Thus, the full potential of ferritin metal-binding sites for catalysis and protein-controlled nanoparticle growth remains to be reached.

1.6.1 Nanomaterials Synthesized in Ferritins

The oldest use of ferritin cages in nanochemistry has been as a nanomaterial template [3, 4, 67]. When used to template nanomaterials, cations enter the cavity through the ion entry channels (Figs. 1.1, 1.4) and self-assemble into materials inside the protein cage. Ferritin protein nanocages contain arrays of ion channels, which, because of the protein properties, are uniquely soluble in aqueous solvents, contrasting with the related membrane ion channel proteins. Disassembled/reassembled ferritin cages have been used to encapsulate a DNA probe and fluorescence reporters for picomolar bioassays and immunoassays [3, 4].

Among the materials made using ferritin protein nanocage templates are semiconductors (CdS nanodots) gold nanospheres, and a variety of iron particles with magnetic properties [3, 4, 67]; such iron minerals when used for imaging are likely dissolved by the biological pathways for natural ferritin iron biominerals.

When ferritin protein cages are used as a template, the uniform nanoparticles are limited by the interior cavity of the protein cage. Thus, the sizes are <8 nm diameter when 24 subunit, maxi-ferritin cages from bacteria, plants, and animals are used; and <5 nm in diameter when 12 subunit mini-ferritin cages are used (See Section 1.2). Ferritin templates for larger structures have been developed by modification of cage surface residue that enhance ferritin aggregation [3, 4, 67] by stabilization of 3D ferritin crystals with silica in the interstitial spaces of the protein crystals [73], or as 2D lattices on various substrates or aggregates, for example, [74, 75]. When empty ferritin protein cages are used as starting material, they are sometimes called "apoferritin" because they have no mineral. Variant protein cages for templating are produced as recombinant proteins from wild-type mammalian sequences. Negatively charged amino acids, naturally on the interior of the cage/surface of the cavity, create local cation concentrations high enough to initiate nanoparticle formation. In some cases design changes that facilitate metal binding are introduced by protein engineering, exemplified by the production of silver and gold nanoparticles inside ferritin [76].

The outer surfaces of ferritin cages have also been recruited for nanosyntheses, for example, [77]. Here, negatively charged caged residues normally on the outside of a mini-ferritin protein cage from the bacterium *Listeria innocua* were made available as a templating surface by turning the cage "inside out" using immobilization, two-step modifications, and elution techniques. Other approaches use modifications of the outer surface. The wide range of amino acid sequences available among ferritin protein cages, which can vary as much as 80% [9], as well as the two different cages sizes, indicate the vast untapped potential of ferritins cages in nanoparticle synthesis.

1.6.2 Ferritin Protein Cages in Metalloorganic Catalysis and Nanoelectronics

Ferritin protein nanocages have been used as catalysts to produce polymers of defined molecular weight, with a narrow size distribution. Palladium and rhuthenium metalloorganic complexes bind at amino acid side chains in the cage, for example, [5, 65, 66]. Changes in organic metallic binding densities, stabilities, and location have recently been achieved with engineered amino acid substitutions, such as selective insertion of cysteine or histidine, especially on the interior surfaces of the cage, facing the cavity. Reactants diffuse through the ferritin protein cage to the nanocavity (Fig. 1.1) where polymerization occurs. Manipulation of ferritin protein cage pore/channels to enhance reactant entry through pore unfolding by amino acid substitutions or with added chaotropes [7] or to control polymer properties using modified eukaryotic sites/extrusion channels for controlled polymerization order and crystallinity are subjects for future exploration and development.

Larger, inorganic catalysts synthesized inside ferritin nanocages have been used to produce with a variety of spatial distributions. In this approach, empty protein cages are distributed in the desired array using surface properties of the protein [6]. Then catalytic nanoparticles are produced inside the cages. Next, the protein cages are selectively removed leaving the nanoparticles exposed. Finally, the nanoparticles deposited in arrays controlled by ferritin protein cage properties catalyze carbon nanotube growth in arrays determined by the controlled pattern of ferritin deposition. Single Pt nanoparticles, synthesized inside ferritin and embedded inside NiO film, have demonstrated low power and stable operation in a memory cell [69]. Future manipulations of ferritin cage surface structure should expand an array of deposition possibilities, and manipulation of ferritin protein natural metal-binding sites should produce more selective control of synthesized nanoparticle properties.

1.6.3 Imaging and Drug Delivery Agents Produced in Ferritins

Entrapment inside ferritin protein cages has been used to deliver hydrophilic drugs, imaging agents such as fluorophores radionuclides, nuclear medicine such as ^{177}Lu, ^{90}Y, and antitumor drugs such as doxorubicin [3, 4, 67], cisplatin, carboplatin, and ozaloplatin [78]. Dissociation/association of ferritin protein cages at low/high pH has also been used to trap DNA probes or probes for bioassay and immunoassay at picomolar concentrations [3].

Recently, modified ferritin targeted to alpha-v beta-3 integrins have found use in imaging vascular inflammation and angiogenesis, and influencing metabolism in C32 human melanoma cells [79]. Ferritin-containing magnetic nanoparticles or conjugated to Cy5.5 has been successfully used to the image cells (vascular macrophages) by magnetic resonance or fluorescence that are key to understanding atherosclerotic plaques and heart disease [80].

The natural ability of living cells to selectively recognize and incorporate exogenous ferritin [38, 81, 82] reflect the intrinsic and complex surfaces of ferritin protein cages that themselves are only beginning to be understood [1]. Coupled with modifications of ferritin protein cages that modulate interactions with specific disease cells,

the vast potential of using ferritin protein cages lies mostly untapped in nanomedicine. Further, the emphasis of many ferritin-based nanomaterial studies on L subunit maxi-ferritin without active sites, or mini-ferritins (Dps proteins) with active sites on the inner cage surface, leaves underutilized ferritin protein-based control of mineral nucleation and growth associated with buried catalytic sites and mineral nucleation channels (Section 1.4, Fig. 1.5). Exploitation of the inherent properties of H ferritin protein cages that influence the order of ferritin nanomineral in Nature remains for future development of ferritin-based synthetic nanomaterials.

1.7 SUMMARY AND PERSPECTIVES

Ferritins are water-soluble, highly symmetrical, protein nanocages with ion channels for Fe(II) entry to Fe/O oxidoreductase sites that initiate the synthesis of hydrated ferric oxide minerals inside large (60% v/v) cage cavities. The protein-caged, iron biominerals provide required intracellular iron concentrates for cell growth and division. Ancient in origin, ferritins self-assemble from four α-helix bundle protein subunits to achieve a very stable structure that is soluble in aqueous solvents. Each funnel-shaped ion channel in ferritin cages has external pores and directs ferrous substrate through the cage to multiple protein oxidoreductase sites that initiate biomineral nucleation; ferrous ion exit from dissolved ferritin biomineral also occurs through the external pores ion channels, dependent on a different set of residues than ion entry. Recent identification in ferritin protein cages of sites that control mineral order/crystallinity (nucleation channels) provides a new design dimension for ferritin-based nanotechnology.

Current uses of ferritin protein nanocages in nanotechnology are as follows: templates for nanomaterials, arrays used in nanodevice production, catalysts for nanopolymer synthesis, reagents for cellular imaging and picomole bioanalytical chemistry; these use ferritin protein cages in relatively native states.

Design modifications have mainly been of nonconserved residues for catalysts binding or cell recognition. An exciting frontier is the modification of ferritin functional subdomains, such as the external pores, ion channels, and protein-based mineral nucleation/crystallization controls to increase the sophistication of ferritin-based nanomaterials, nanocatalysts, and nanodevices. Nature has manipulated ferritin protein cages to produce iron particles with defined properties. Scientists have just begun to explore the potential of engineered ferritin protein cages in nanotechnology.

ACKNOWLEDGMENTS

The authors are grateful for the financial support of the NIH and the CHORI Foundation during the preparation of this chapter and the intellectual contributions of colleagues and members of the Theil Group.

REFERENCES

[1] Theil, E. C. *Curr. Opin. Chem. Biol.* **2011**, *15*, 304–311.

[2] Mann, S. *Nat. Mater.* **2009**, *8*, 781–792.

[3] Maham, A.; Tang, Z.; Wu, H.; Wang, J.; Lin, Y. *Small* **2009**, *5*, 1706–1721.

[4] Uchida, M.; Kang, S.; Reichhardt, C.; Harlen, K.; Douglas, T. *Biochim. Biophys. Acta* **2010**, *1800*, 834–845.

[5] Takezawa, Y.; Bockmann, P.; Sugi, N.; Wang, Z.; Abe, S.; Murakami, T.; Hikage, T.; Erker, G.; Watanabe, Y.; Kitagawa, S.; Ueno, T. *Dalton Trans.* **2011**, *40*, 2190–2195.

[6] Yamashita, I.; Iwahori, K.; Kumagai, S. *Biochim. Biophys. Acta* **2010**, *1800*, 846–857.

[7] Liu, X.; Jin, W.; Theil, E. C. *Proc. Natl. Acad. Sci. USA* **2003**, *100*, 3653–3658.

[8] Theil, E. C.; Goss, D. J. *Chem. Rev.* **2009**, *109*, 4568–4579.

[9] Bevers, L. E.; Theil, E. C. Maxi- and mini-ferritins: minerals and protein nanocages. In *Progress in Molecular and Subcellular Biology*; Muller, W. E. G., Ed.; Springer-Verlag: Berlin-Heidelberg, **2011**; pp 18.

[10] Liu, X.; Theil, E. C. *Acc. Chem. Res.* **2005**, *38*, 167–175.

[11] Crichton, R. R.; Declercq, J. P. *Biochim. Biophys. Acta* **2010**, 1800, 706–718.

[12] Tosha, T.; Ng, H. L.; Bhattasali, O.; Alber, T.; Theil, E. C. *J. Am. Chem. Soc.* **2010**, *132*, 14562–14569.

[13] Turano, P.; Lalli, D.; Felli, I. C.; Theil, E. C.; Bertini, I. *Proc. Natl. Acad. Sci. USA* **2010**, *107*, 545–550.

[14] Ilari, A.; Stefanini, S.; Chiancone, E.; Tsernoglou, D. *Nat. Struct. Biol.* **2000**, *7*, 38–43.

[15] Chiancone, E.; Ceci, P. *Biochim. Biophys. Acta* **2010**, *1800*, 798–805.

[16] Takagi, H.; Shi, D.; Ha, Y.; Allewell, N. M.; Theil, E. C. *J. Biol. Chem.* **1998**, *273*, 18685–18688.

[17] Theil, E. C.; Liu, X. S.; Tosha, T. *Inorganica Chim. Acta* **2008**, *361*, 868–874.

[18] Banyard, S. H.; Stammers, D. K.; Harrison, P. M. *Nature* **1978**, *271*, 282–284.

[19] Stefanini, S.; Desideri, A.; Vecchini, P.; Drakenberg, T.; Chiancone, E. *Biochemistry* **1989**, *28*, 378–382.

[20] Jiang, Y.; Lee, A.; Chen, J.; Ruta, V.; Cadene, M.; Chait, B. T.; MacKinnon, R. *Nature* **2003**, *423*, 33–41.

[21] Douglas, T.; Ripoll, D. R. *Protein Sci.* **1998**, *7*, 1083–1091.

[22] Takahashi, T.; Kuyucak, S. *Biophys. J.* **2003**, *84*, 2256–2263.

[23] Levi, S.; Santambrogio, P.; Corsi, B.; Cozzi, A.; Arosio, P. *Biochem. J.* **1996**, *317 (Pt 2)*, 467–473.

[24] Haldar, S.; Bevers, L. E.; Tosha, T.; Theil, E. C. *J. Biol. Chem.* **2011**, *286*, 25620–25627.

[25] Bellapadrona, G.; Stefanini, S.; Zamparelli, C.; Theil, E. C.; Chiancone, E. *J. Biol. Chem.* **2009**, *284*, 19101–19109.

[26] Lawson, D. M.; Artymiuk, P. J.; Yewdall, S. J.; Smith, J. M.; Livingstone, J. C.; Treffry, A.; Luzzago, A.; Levi, S.; Arosio, P.; Cesareni, G.; Thomas, C. D.; Shaw, W. D.; Harrison, P. M. *Nature* **1991**, *349*, 541–544.

[27] Toussaint, L.; Bertrand, L.; Hue, L.; Crichton, R. R.; Declercq, J. P. *J. Mol. Biol.* **2007**, *365*, 440–452.

[28] Barnes, C. M.; Theil, E. C.; Raymond, K. N. *Proc. Natl. Acad. Sci. USA* **2002**, *99*, 5195–5200.

[29] Ha, Y.; Shi, D.; Small, G. W.; Theil, E. C.; Allewell, N. M. *J. Biol. Inorg. Chem.* **1999**, *4*, 243–256.

[30] Treffry, A.; Zhao, Z.; Quail, M. A.; Guest, J. R.; Harrison, P. M. *Biochemistry* **1995**, *34*, 15204–15213.

[31] Fetter, J.; Cohen, J.; Danger, D.; Sanders-Loehr, J.; Theil, E. C. *J. Biol. Inorg. Chem.* **1997**, *2*, 652–661.

[32] Bou-Abdallah, F.; Papaefthymiou, G. C.; Scheswohl, D. M.; Stanga, S. D.; Arosio, P.; Chasteen, N. D. *Biochem. J.* **2002**, *364*, 57–63.

[33] Pereira, A. S.; Small, W.; Krebs, C.; Tavares, P.; Edmondson, D. E.; Theil, E. C.; Huynh, B. H. *Biochemistry* **1998**, *37*, 9871–9876.

[34] Moënne-Loccoz, P.; Krebs, C.; Herlihy, K.; Edmondson, D. E.; Theil, E. C.; Huynh, B. H.; Loehr, T. M. *Biochemistry* **1999**, *38*, 5290–5295.

[35] Krebs, C.; Bollinger, J. M., Jr.; Theil, E. C.; Huynh, B. H. *J. Biol. Inorg. Chem.* **2002**, *7*, 863–869.

[36] Bollinger, J. M.; Krebs, C.; Vicol, A.; Chen, S.; Ley, B. A.; Edmondson, D. E.; Huynh, B. H. *J. Am. Chem. Soc.* **1998**, *120*, 1094–1095.

[37] Tinberg, C. E.; Lippard, S. J. *Acc. Chem. Res.* **2011**, *44*, 280–288.

[38] Li, L.; Fang, C. J.; Ryan, J. C.; Niemi, E. C.; Lebron, J. A.; Bjorkman, P. J.; Arase, H.; Torti, F. M.; Torti, S. V.; Nakamura, M. C.; Seaman, W. E. *Proc. Natl. Acad. Sci. USA* **2011**, *107*, 3505–3510.

[39] Moenne-Loccoz, P.; Krebs, C.; Herlihy, K.; Edmondson, D. E.; Theil, E. C.; Huynh, B. H.; Loehr, T. M. *Biochemistry* **1999**, *38*, 5290–5295.

[40] Hwang, J.; Krebs, C.; Huynh, B. H.; Edmondson, D. E.; Theil, E. C.; Penner-Hahn, J. E. *Science* **2000**, *287*, 122–125.

[41] Nordlund, P.; Eklund, H. *Curr. Opin. Chem. Biol.* **1995**, *5*, 758–766.

[42] Schwartz, J. K.; Liu, X. S.; Tosha, T.; Theil, E. C.; Solomon, E. I. *J. Am. Chem. Soc.* **2008**, *130*, 9441–9450.

[43] Liu, X.; Theil, E. C. *Proc. Natl. Acad. Sci. USA* **2004**, *101*, 8557–8562.

[44] Tosha, T.; Hasan, M. R.; Theil, E. C. *Proc. Natl. Acad. Sci. USA* **2008**, *105*, 18182–18187.

[45] Bou-Abdallah, F.; Zhao, G.; Mayne, H. R.; Arosio, P.; Chasteen, N. D. *J. Am. Chem. Soc.* **2005**, *127*, 3885–3893.

[46] Bou-Abdallah, F.; McNally, J.; Liu, X. X.; Melman, A. *Chem. Commun.* **2011**, *47*, 731–733.

[47] Jameson, G. N.; Jin, W.; Krebs, C.; Perreira, A. S.; Tavares, P.; Liu, X.; Theil, E. C.; Huynh, B. H. *Biochemistry* **2002**, *41*, 13435–13443.

[48] Waldo, G. S.; Theil, E. C. Ferritin and Iron Biomineralization. In *Comprehensive Supramolecular Chemistry, Bioinorganic Systems, Vol. 5*; Suslick, K. S., Ed.; Pergamon Press: Oxford, UK, **1996**; pp 65–89.

[49] Mertz, J. R.; Theil, E. C. *J. Biol. Chem.* **1983**, *258*, 11719–11726.

[50] May, C. A.; Grady, J. K.; Laue, T. M.; Poli, M.; Arosio, P.; Chasteen, N. D. *Biochim. Biophys. Acta* **2010**, *1800*, 858–870.

[51] Gould, S. B.; Waller, R. F.; McFadden, G. I. *Annu. Rev. Plant Biol.* **2008**, *59*, 491–517.

[52] Wade, V. J.; Treffry, A.; Laulhere, J.-P.; Bauminger, E. R.; Cleton, M. I.; Mann, S.; Briat, J.-F.; Harrison, P. M. *Biochim. Biophys. Acta* **1993**, *1161*, 91–96.

[53] Waldo, G. S.; Wright, E.; Whang, Z. H.; Briat, J. F.; Theil, E. C.; Sayers, D. E. *Plant Physiol.* **1995**, *109*, 797–802.

[54] Pierre, T. St.; Tran, K. C.; Webb, J.; Macey, D. J.; Heywood, B. R.; Sparks, N. H.; Wade, V. J.; Mann, S.; Pootrakul, P. *Biol. Met.* **1991**, *4*, 162–165.

[55] Andrews, S. C.; Brady, M. C.; Treffry, A.; Williams, J. M.; Mann, S.; Cleton, M. I.; de Bruijn, W.; Harrison, P. M. *Biol. Met.* **1988**, *1*, 33–42.

[56] Moore, G. R.; Mann, S.; Bannister, J. V. *J. Inorg. Biochem.* **1986**, *28*, 329–336.

[57] Zhao, G. *Biochim Biophys Acta* **2010**, *1800*, 815–823.

[58] Aitken-Rogers, H.; Singleton, C.; Lewin, A.; Taylor-Gee, A.; Moore, G. R.; Le Brun, N. E. *J. Biol. Inorg. Chem*. **2004**, *9*, 161–170.

[59] Cozzi, A.; Corsi, B.; Levi, S.; Santambrogio, P.; Biasiotto, G.; Arosio, P. *Blood* **2004**, *103*, 2377–2383.

[60] De Domenico, I.; Ward, D. M.; Kaplan, J.; *Blood* **2009**, *114*, 4546–4551.

[61] Hasan, M. R.; Tosha, T.; Theil, E. C. *J. Biol. Chem.* **2008**, *283*, 31394–31400.

[62] Jin, W.; Takagi, H.; Pancorbo, B.; Theil, E. C. *Biochemistry* **2001**, *40*, 7525–7532.

[63] Liu, X. S.; Patterson, L. D.; Miller, M. J.; Theil, E. C. *J. Biol. Chem.* **2007**, *282*, 31821–31825.

[64] Tosha, T.; Behera, R. K.; Ng, H.-L.; Bhattasali, O.; Alber, T.; Theil, E. C. *J. Biol. Chem.* **2012**, *287*, 13016–13025.

[65] Wang, Z.; Takezawa, Y.; Aoyagi, H.; Abe, S.; Hikage, T.; Watanabe, Y.; Kitagawa, S.; Ueno, T. *Chem. Commun.* **2011**, *47*, 170–172.

[66] Abe, S.; Hirata, K.; Ueno, T.; Morino, K.; Shimizu, N.; Yamamoto, M.; Takata, M.; Yashima, E.; Watanabe, Y. *J. Am. Chem. Soc.* **2009**, *131*, 6958–6960.

[67] Flenniken, M. L.; Uchida, M.; Liepold, L. O.; Kang, S.; Young, M. J.; Douglas, T. *Curr. Top. Microbiol. Immunol.* **2009**, *327*, 71–93.

[68] Iwahori, K.; Yamashita, I. *Nanotechnology* **2008**, *19*, 495601.

[69] Kobayashi, M.; Kumagai, S.; Zheng, B.; Uraoka, Y.; Douglas, T.; Yamashita, I. *Chem. Commun.* **2011**, *47*, 3475–3477.

[70] Santambrogio, P.; Levi, S.; Arosio, P.; Palagi, L.; Vecchio, G.; Lawson, D. M.; Yewdall, S. J.; Artymiuk, P. J.; Harrison, P. M.; Jappelli, R. *J. Biol. Chem.* **1992**, *267*, 14077–14083.

[71] Wong, K. K.; Colfen, H.; Whilton, N. T.; Douglas, T.; Mann, S. *J. Inorg. Biochem.* **1999**, *76*, 187–195.

[72] Liu, G.; Wang, J.; Wu, H.; Lin, Y. *Anal. Chem.* **2006**, *78*, 7417–7423.

[73] Lambert, E. M.; Viravaidya, C.; Li, M.; Mann, S. *Angew. Chem. Int. Ed.* **2010**, *49*, 4100–4103.

[74] Srivastava, S.; Samanta, B.; Jordan, B. J.; Hong, R.; Xiao, Q.; Tuominen, M. T.; Rotello, V. M. *J. Am. Chem. Soc.* **2007**, *129*, 11776–11780.

[75] Saha, K.; Bajaj, A.; Duncan, B.; Rotello, V. M. *Small* **2011**, *7*, 1903–1918.

[76] Butts, C. A.; Swift, J.; Kang, S. G.; Di Costanzo, L.; Christianson, D. W.; Saven, J. G.; Dmochowski, I. J. *Biochemistry* **2008**, *47*, 12729–12739.

[77] Suci, P. A.; Kang, S.; Young, M.; Douglas, T. *J. Am. Chem. Soc.* **2009**, *131*, 9164–9165.

[78] Yang, Z.; Wang, X.; Diao, H.; Zhang, J.; Li, H.; Sun, H.; Guo, Z. *Chem. Commun*. **2007**, 3453–3455.

[79] Kitagawa, T.; Kosuge, H.; Uchida, M.; Dua, M. M.; Iida, Y.; Dalman, R. L.; Douglas, T.; McConnell, M. V. *Mol. Imaging Biol.* **2011**.

[80] Terashima, M.; Uchida, M.; Kosuge, H.; Tsao, P. S.; Young, M. J.; Conolly, S. M.; Douglas, T.; McConnell, M. V. *Biomaterials* **2011**, *32*, 1430–1437.

[81] San Martin, C. D.; Garri, C.; Pizarro, F.; Walter, T.; Theil, E. C.; Nunez, M. T. *J. Nutr*. **2008**, *138*, 659–666.

[82] Li, J. Y.; Paragas, N.; Ned, R. M.; Qiu, A.; Viltard, M.; Leete, T.; Drexler, I. R.; Chen, X.; Sanna-Cherchi, S.; Mohammed, F.; Williams, D.; Lin, C. S.; Schmidt-Ott, K. M.; Andrews, N. C.; Barasch, J. *Dev. Cell* **2009**, *16*, 35–46.